Available online at www.sciencedirect.com
SCIENCE DIRECT
Journal of Catalysis 226 (2004) 422–434
JOURNAL OF CATALYSIS
www.elsevier.com/locate/jcat

A transient in situ FTIR and XANES study of CO oxidation over Pt/Al_2O_3 catalysts

Per-Anders Carlsson [a,b,c,*], Lars Österlund [a,c,e], Peter Thormählen [a,c], Anders Palmqvist [a,d], Erik Fridell [a,c], Jonas Jansson [a,b,1], Magnus Skoglundh [a,d]

[a] *Competence Centre for Catalysis, Chalmers University of Technology, SE-412 96 Göteborg, Sweden*
[b] *Department of Chemical Engineering and Environmental Sciences, Chalmers University of Technology, SE-412 96 Göteborg, Sweden*
[c] *Department of Applied Physics, Chalmers University of Technology, SE-412 96 Göteborg, Sweden*
[d] *Department of Materials and Surface Chemistry, Chalmers University of Technology, SE-412 96 Göteborg, Sweden*
[e] *Department of Environment and Protection, FOI NBC Defense, SE-901 82 Umeå, Sweden*

Received 4 March 2004; revised 4 June 2004; accepted 7 June 2004

Available online 20 July 2004

Abstract

We report experimental results for the oxidation of CO over supported Pt/Al_2O_3 catalysts operating in oxygen excess at atmospheric pressure. To study the reaction kinetics under transient conditions we have employed step changes of the O_2 concentration by intermittently switching off the O_2 supply at various temperatures ranging from 523 to 623 K. Detailed in situ FTIR and XANES data for CO coverage and the chemical state of Pt, respectively, are presented together with the CO conversion, which in both cases was monitored by mass spectrometry. A red-shift of the vibrational frequency of linearly bonded CO which correlates with a blue-shift of the Pt L_{III} binding energy indicates that the Pt catalyst initially is partially oxidised and gradually reduced when the O_2 supply is switched off. Control experiments with a NO_2 oxidised Pt/Al_2O_3 catalyst support these findings. A hysteresis in the catalytic activity due to the different rates whereby Pt is oxidised and reduced as a function of gas-phase composition is observed. The activation energy for the Pt oxide reduction (decomposition) process is estimated to be about 50 kJ/mol. The results further emphasise that the conventional three-step Langmuir–Hinshelwood (LH) scheme used to interpret CO oxidation on Pt surfaces must be complemented by a Pt oxidation and reduction mechanism during transient conditions. Moreover, FTIR data suggest that during the extinction, the partially oxidised platinum surface is reduced by chemisorbed CO which should be explicitly accounted for in the modeling of the reaction mechanism.

Keywords: Catalysis; Ignition; Extinction; CO oxidation; Platinum; Platinum oxide; Pt/Al_2O_3; Step-response experiments; FTIR; XANES

1. Introduction

The oxidation of carbon monoxide over precious metals, e.g., platinum, is probably one of the most studied catalytic reactions, beginning already with the pioneering work by Langmuir in 1922 [1]. The role as a key step in many industrial processes and the importance in pollution control for stationary and mobile applications [2] motivates further studies of this reaction. Even though the literature on the subject is extensive, there is still a need to further clarify the reaction mechanism, particularly under transient conditions, e.g., ignition and extinction.

It is well documented that under UHV conditions, the CO oxidation on Pt proceeds via the conventional three-step Langmuir–Hinshelwood (LH) reaction scheme [3,4],

$$CO_{gas} \rightleftarrows CO_{ads}, \quad (1)$$

* Corresponding author.
E-mail address: perc@chemeng.chalmers.se (P.-A. Carlsson).
[1] Present address. Volvo Powertrain Dept 24446, BC2 SE-405 08 Göteborg, Sweden.

0021-9517/$ – see front matter
doi:10.1016/j.jcat.2004.06.009

$$(O_2)_{gas} \rightarrow 2O_{ads}, \quad (2)$$

$$CO_{ads} + O_{ads} \rightarrow (CO_2)_{gas}, \quad (3)$$

where the indices "gas" and "ads" refer to gas phase and adsorbed species, respectively. Here CO adsorbs associatively and starts to desorb rapidly above about 350 K, while O_2 adsorbs dissociatively above about 100 K [5] and desorbs associatively above 720 K [6]. CO diffuses rapidly over the surface and reacts with O to yield CO_2, which immediately desorbs into the gas phase (CO_2 desorbs at 95 K [7]).

Based on the reaction scheme (1)–(3) one can predict, in agreement with experiments, two stable states for CO oxidation [4,8,9]. One state (branch) with a low reaction rate and one with high reaction rate. Physically this can be traced to the different adsorption kinetics of CO and O_2; CO and O_2 adsorb competitively, where CO adsorption is favored at low temperatures. This together with the ability for CO molecules to form rather dense adsorption layers, blocking O_2 adsorption, leads to low reaction rates when the CO/O_2 ratio is too high.

In the state with a low reaction rate, the Pt surface is predominantly CO covered (the reaction is CO self-poisoned), while in the state with a high reaction rate, it is almost exclusively covered with O species. The two reaction-rate branches overlap giving rise to a bistable regime for which the actual reaction rate (high or low) depends not only on the reaction conditions but also on the preceding history of the system [4,8,9]. Moreover, the exact location and form of the bistable regime are a function of reaction conditions. For example, with increasing temperature and/or decreasing CO/O_2 ratio, the tendency for CO self-poisoning relents and shrinks the bistable regime. A temperature increase shifts the CO adsorption–desorption equilibrium towards desorption, leaving a larger part of the active surface available for O_2 adsorption.

Often the transitions between the two (high and low) reaction rate branches are referred to as ignition and extinction, respectively. Strictly speaking this is only the case when the so-called Frank–Kamenetskii condition is not fulfilled [11], i.e., when the ability of the Pt catalyst to dissipate heat is not sufficient to avoid a reaction-induced heating (temperature rise). These are thus not solely kinetic effects. In those cases when one can expect that the kinetics alone governs the transitions, e.g., where full conversion is not realised or under low partial pressures of reactants, or when the heat dissipation is effective, the "ignition" and "extinction" processes should more correctly be referred to as kinetic phase transitions, with bifurcations connecting the two stable reaction-rate branches [8]. In this study we have not determined the conditions of the transitions in detail, since this is not important for a qualitative interpretation of the data, and we do not distinguish between a kinetic-phase transition and ignition/extinction, respectively.

A special feature of the CO oxidation over Pt is the occurrence of intrinsic kinetic rate oscillations, under otherwise constant reaction conditions, leading to an oscillating CO_2 production rate. The first observation of such oscillations was reported by Hugo in 1970 [12]. The nature of these oscillations is not yet fully understood. It is, however, clear that some slow process, i.e., slow in comparison with reactions (1)–(3), must accompany the LH reaction scheme above in order to periodically move the system between the two reaction rate branches. On Pt(110) and Pt(100) the oscillations apparent under vacuum conditions can be traced to a reversible surface reconstruction, which exposes surfaces with very different O_2 sticking probabilities while on Pt(111), for which no surface reconstruction exists, no oscillations are observed [4]. However, under atmospheric conditions, oscillations may occur irrespective of exposed platinum facet. The incorporation of a Pt oxidation and reduction cycle as suggested by Sales et al. [13] is generally considered as the most likely mechanism to explain such oscillations [14]. In this model a less active (or non-active) surface oxide is proposed to form under oxygen-rich conditions, which eventually brings the system from the high to the low reaction-rate branch. The catalytic activity is restored when CO reacts with oxidic oxygen and reduces Pt back to its metallic state, which thus completes the cycle. There are a number of studies which support this model and the existence of an oxide phase [15,16]. Usually, the oxide model incorporates the following processes,

$$O_{ads} \rightleftarrows O_{ox}, \quad (4)$$

$$CO_{ads} + O_{ox} \rightarrow (CO_2)_{gas}, \quad (5)$$

where the index "ox" refers to an oxidised Pt site. It is, however, not clear if the formation of O_{ox} is governed solely by Eq. (4) or whether O_2 dissociation on the oxide phase (e.g., at vacancies) also occurs, viz.

$$(O_2)_{gas} \rightarrow 2O_{ox}. \quad (6)$$

Previous studies of CO oxidation over supported platinum catalysts at atmospheric pressures reported by our group [10,17] have shown that the conventional LH reaction scheme can be used to successfully model the ignition process, i.e., the transition from the low to the high reaction rate branch as the CO/O_2 ratio is decreased. Based on mean-field kinetic equations combined with suitable reactor equations, the gas-phase concentrations, gas-phase and catalyst temperatures, and surface coverages were possible to predict with simulations for both Pt/Al_2O_3 monolith samples [17] and planar electron-beam lithography (EBL) fabricated Pt/SiO_2 model catalysts [10]. However, using the same equations to simulate the extinction process, that is the reversed transition from the high to the low reaction-rate branch as the CO/O_2 ratio is increased, was not possible without changing the model parameters, e.g., the sticking probability for O_2 or introducing a significantly lower CO + O reaction rate [10,17]. Interpreting these findings, one should keep in mind the so-called material and structure gaps between single crystals under UHV conditions and supported catalysts at atmospheric pressure. Although the (111) and (100) facets are the dominating surfaces for supported platinum

particles under "working conditions" [18], there is still a boundary between the Pt particle and the support, characteristic for such catalysts. High pressures give effects like high surface coverages which in turn may lead to significant adsorbate-adsorbate [19] or adsorbate-surface interactions. Nevertheless, it is natural to complement these studies and incorporate platinum oxidation and reduction explicitly, i.e., reactions (4) and (5). Specifically, our aim in this paper is to provide experimental support and mechanistic understanding of the oxide reduction during the extinction process described above. To this end we employ different in situ techniques, i.e., FTIR and XANES both in combination with on-line mass spectrometry, to monitor the surface coverage, chemical state and CO conversion of a Pt/Al_2O_3 catalyst during CO oxidation.

2. Experimental

2.1. Catalyst preparation

The catalyst support material, γ-Al_2O_3, was prepared by calcining boehmite (Disperal, Sasol) in air at 873 K for 8 h. The formed alumina phase was sieved and the 125 to 210 µm fraction was used for further preparation. This fraction was dispersed in distilled water and the pH was adjusted to 10.5 by ammonia addition (NH_4OH solution, Riedel–de Haën). An aqueous platinum hydroxide solution (tetraammineplatinum(II)hydroxide, Johnson Matthey) was added dropwise to the alumina slurry under continuous stirring to yield a platinum loading of 2.0 wt%. The slurry was then kept under continuous stirring for 1 h, frozen with liquid nitrogen, freeze-dried, and finally calcined in air at 873 K for 1.5 h. The chemisorbed amount of CO (Micrometrics, ASAP2010C) at 300 K was 16.0 µmol/g sample which corresponds to a platinum dispersion of 22%, assuming 0.7 CO molecules chemisorbed per surface platinum atom [20]. The BET surface area was measured to be 157 m^2/g.

2.2. In situ FTIR spectroscopy

The time resolved in situ FTIR spectroscopy experiments were performed in diffuse reflectance mode with a Bio-Rad FTS6000 spectrometer equipped with a Harrick Praying Mantis DRIFT reaction cell. Gases were introduced with individual mass-flow controllers into two different streams which were connected to a four-port switching valve positioned close to the reactor chamber in the DRIFT cell. This configuration facilitates fast switching between the two gas streams, allowing one stream to enter the reactor while the other is ventilated or vice versa. In all experiments high-purity gases were used ($H_2O < 3$, $O_2 < 2$, $CH < 0.5$, $CO < 0.5$, and $H_2 < 0.1$ mol ppm). The reactor was loaded with 57 mg of a powder mixture containing 50 wt% catalyst diluted in KBr. The sample was initially dried in situ in a 150 ml(NTP)/min Ar flow at 400 K for 12 h before being exposed to different reactant gas compositions. Collection of five IR spectra per second keeping a wavenumber resolution of 1.2 cm^{-1} was possible using a liquid nitrogen cooled MCT detector. The product stream was continuously analysed, following the CO (m/e 28), O_2 (m/e 32), Ar (m/e 40), and CO_2 (m/e 44) signals, with a Balzers Quadstar 422 mass spectrometer. Before each measurement, the sample was pre-treated with a net-oxidising $CO/O_2/Ar$ mixture for 20 min at the actual temperature to be studied (cf. Table 1) and a reference spectrum was collected. By using this routine, the appearance of IR bands from alumina-related carbonates, probably acting as spectators (i.e., species not involved in the catalytic cycle), in the spectra was minimised, thus simplifying the result analysis. Moreover, the reference spectrum will contain no IR bands for CO bonded to Pt, since the CO coverage is low due to the CO + O reaction (net-oxidising mixture). Three different measurement series of the reduction-oxidation processes of the Pt/Al_2O_3 sample due to step changes of the CO/O_2 ratio in the range of 523–623 K were performed (cf. Table 1). In the first series (IR1), a 1.0 vol% CO/5.0 vol% O_2/Ar (from here vol% is denoted with %) mixture was exposed for 60 s, followed by a switch to a 1.0% CO/Ar flow for 300 s (reduction phase) and then switching back to 1.0% CO/5.0% O_2/Ar for another 240 s (oxidation phase). In the second (IR2) and third (IR3) experimental series, 1000 vol ppm (from here denoted with ppm) CO and 1.0% O_2, respectively, were used under otherwise the same conditions. A total gas flow of 150 ml(NTP)/min corresponding to a space velocity of 100,000 h^{-1} was used in all experiments. The pre-treatments and the subsequent

Table 1
Summary of experimental conditions for the IR (IR1-3) and XANES (X1-2) measurements

Experiment	Gas composition	Duration	Process
IR1	1.0 vol% CO/5.0 vol% O_2/Ar	20 min	Pre-treatment
	1.0 vol% CO/5.0 vol% O_2/Ar	60 s	
	1.0 vol% CO/Ar	300 s	Reduction phase
	1.0 vol% CO/5.0 vol% O_2/Ar	240 s	Oxidation phase
IR2	1000 ppm CO/5.0 vol% O_2/Ar	20 min	Pre-treatment
	1000 ppm CO/5.0 vol% O_2/Ar	60 s	
	1000 ppm CO/Ar	300 s	Reduction phase
	1000 ppm CO/5.0 vol% O_2/Ar	240 s	Oxidation phase
IR3	1.0 vol% CO/1.0 vol% O_2/Ar	20 min	Pre-treatment
	1.0 vol% CO/1.0 vol% O_2/Ar	60 s	
	1.0 vol% CO/Ar	300 s	Reduction phase
	1.0 vol% CO/1.0 vol% O_2/Ar	240 s	Oxidation phase
X1	1.0 vol% CO/5.0 vol% O_2/He	10 min	Pre-treatment
	1.0 vol% CO/5.0 vol% O_2/He	120 s	
	1.0 vol% CO/He	280 s	Reduction phase
	1.0 vol% CO/5.0 vol% O_2/He	370 s	Oxidation phase
X2	1.0 vol% CO/5.0 vol% O_2/He	10 min	Pre-treatment
	1.0 vol% CO/5.0 vol% O_2/He	60 s	
	1.0 vol% CO/He	180 s	Reduction phase
	1.0 vol% CO/5.0 vol% O_2/He	170 s	Oxidation phase

The IR1-3 experiments were repeated for 523, 548, 573, 598 and 623 K while the X1 and X2 experiments correspond to 523 and 623 K, respectively.

reduction-oxidation experiments were performed in the order of decreasing temperature attempting to minimise the effects of nonstable carbonates in the IR analysis.

In addition to the CO oxidation experiments (IR1-3) described above, CO adsorption (1% CO/Ar) control measurements were also performed on a reduced sample (treated with 4.0% H_2 at 723 K for 10 min, 150 ml(NTP)/min) at 523 and 623 K. Similarly, CO adsorption on a strongly oxidised sample (treated with 250 ppm NO_2 at 723 K for 10 min, 150 ml(NTP)/min [21]) at 523 and 573 K was also performed.

2.3. In situ XANES

Dispersive Pt L_{III}-edge XANES measurements were performed in transmission mode at beamline ID24 at ESRF in Grenoble, France, on pressed pellets of 100 mg of the Pt/Al_2O_3 sample and 50 mg BN. The Pt L_{III} edge energy was defined as the position of the inflection point of the white line step and is given in absolute binding energy. The pellets were mounted in an in situ temperature controlled flow reactor cell, to which a reactant gas mixture, obtained via separate mass-flow controllers, was introduced. The total flow was 100 ml(NTP)/min corresponding to a space velocity of about 70,000 h^{-1}. The product stream was continuously analysed with a Balzers Prisma mass spectrometer following the m/e 28, 32, 40 and 44 signals. The beamline uses a Si [111] polychromator crystal, operating in Bragg mode, for selection of the desired range of X-ray wavelengths, and a 1152 × 1242 pixel CCD solid-state detector for spectral analysis. Harmonic rejection was achieved through the use of two additional mirrors in the beamline, and the estimated energy resolution was $\Delta E/E \approx 1.2\text{–}1.5 \times 10^{-4}$. The data analysis was performed using the program Delia in the XAID toolbox of the XOP 2.0 software package [22].

The energy scale of the CCD detector was calibrated before and after each measurement series using a Pt metal foil (Puratronics, 99.99% purity) and fitting the measured data points to those of a Pt foil spectrum taken from the database DABAX in the XOP 2.0 package. The average energy and current in the storage ring during the entire series of measurements were 6 GeV and 180 mA, respectively. The XANES spectra were recorded in situ during CO oxidation in 1.0% CO/5.0% O_2/He at 523 and 623 K, analogous to the FTIR experiments (cf. Table 1).

3. Results

3.1. In situ FTIR spectroscopy

The results from the first series of IR experiments (IR1) with 1.0% CO and 5.0% O_2 are presented in Fig. 1. The figure shows the three-dimensional representations of the evolution of the IR bands in the interval 1750–2250 cm^{-1}

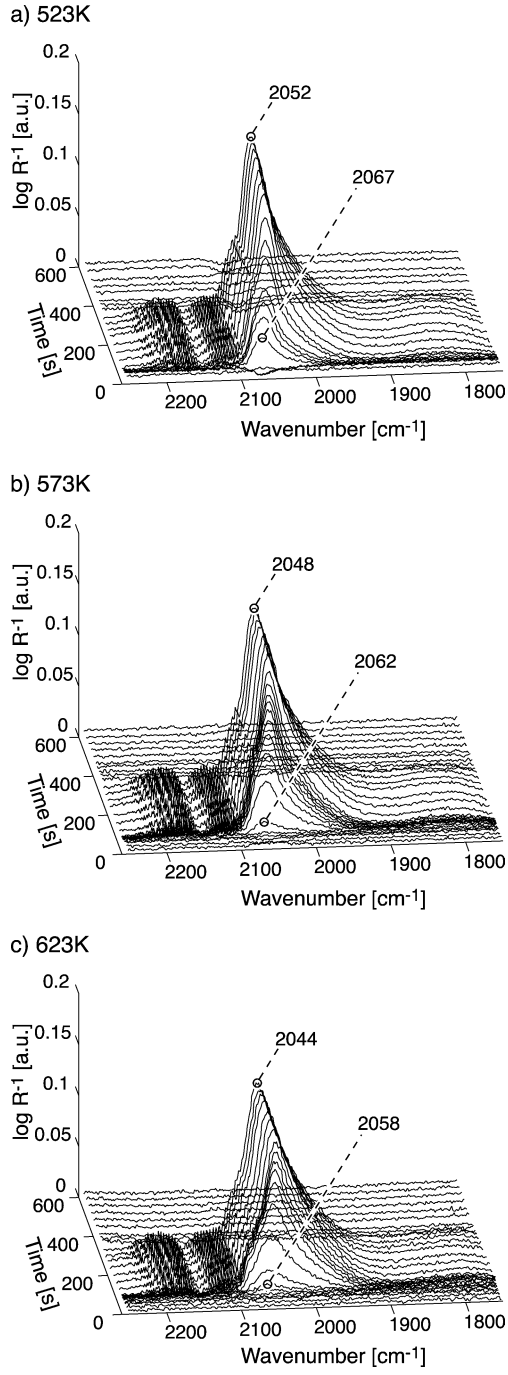

Fig. 1. Evolution of different IR bands in the interval 1750–2250 cm^{-1} for a 2.0% Pt/Al_2O_3 catalyst exposed to 1.0 vol% CO in Ar while switching the O_2 concentration from 5.0 to 0.0 vol% at $t = 60$ s (reduction phase) and then back to 5.0 vol% at $t = 360$ s (oxidation phase) at (a) 523, (b) 573, and (c) 623 K.

(the CO vibrational stretching region) at 523, 573 and 623 K during step changes of the O_2 concentration (cf. Table 1).

The reduction phase is initiated by turning off the O_2 supply at $t = 60$ s. During this phase three main IR bands evolve. The strong band around 2050 cm^{-1} and the weak band around 1825 cm^{-1} correspond to linear bonded CO ($\tilde{\nu}_{lin}^{CO}$) and bridge-bonded CO ($\tilde{\nu}_{br}^{CO}$) on platinum, respec-

Table 2
Summary of the $\tilde{\nu}_{lin}^{CO}$ band shifts, obtained during the reduction of a 2% Pt/Al_2O_3 catalyst, and fitted positions for the $\tilde{\nu}_{lin}^{CO}(Pt^{\delta+})$ band at 523–623 K

Temperature (K)	$\tilde{\nu}_{lin}^{CO}$ (cm^{-1})	$\tilde{\nu}_{lin}^{CO}(Pt^{\delta+})$ (cm^{-1})
523	2067 → 2052	2066
548	2066 → 2050	2063
573	2062 → 2048	2063
598	2062 → 2046	2061
623	2058 → 2044	2054

tively [23–28]. The double band centered around 2144 cm^{-1} corresponds to gaseous CO ($\tilde{\nu}_{gas}^{CO}$) [29]. Into each experiment the $\tilde{\nu}_{lin}^{CO}$ band appears with an initial time lag, relative the gas switch, which will be discussed in detail below. During the reduction phase, a shift of about 15 cm^{-1} toward lower wavenumbers (i.e., red-shift) can be observed for the $\tilde{\nu}_{lin}^{CO}$ band at all temperatures, see also Table 2. Moreover, the $\tilde{\nu}_{lin}^{CO}$ band shifts to lower wavenumbers as the temperature is increased. In contrast to the red-shift of $\tilde{\nu}_{lin}^{CO}$ occurring during the reduction phase at constant temperature, this simply reflects the effect of decreased repulsive CO–CO adsorbate interactions with decreasing CO coverage (the CO saturation coverage is lower at higher temperatures) [26,30]. During the same period, a continuous increase of the $\tilde{\nu}_{br}^{CO}$ and $\tilde{\nu}_{gas}^{CO}$ band intensities towards stationary levels occurs. No wavenumber shifts for the $\tilde{\nu}_{br}^{CO}$ can be observed. The fact that the $\tilde{\nu}_{gas}^{CO}$ band appears simply tells us that the relative gas-phase concentration of CO increases, since the reaction rate, i.e., step (3), diminishes and the consumption of CO ceases.

In order to compare the results obtained in the IR1 experiments with comparable experiments for substantially reduced and oxidised catalysts, CO adsorption (1% CO/Ar) was performed on H_2 and NO_2 pretreated catalysts, respectively, at different temperatures (a reduced Pt/Al_2O_3 catalyst in pure Ar flow was used as IR reference in these experiments). The CO adsorption on a H_2-reduced sample at 523 and 623 K resulted in a 5 cm^{-1} shift of the $\tilde{\nu}_{lin}^{CO}$ towards higher wavenumbers, i.e., blue-shift (not shown). This blue-shift is due to repulsive CO–CO interactions in agreement with previous reports [26,30]. In contrast, the same CO adsorption procedure on a NO_2-oxidised sample showed three different IR absorption bands besides the $\tilde{\nu}_{gas}^{CO}$, as can be seen in Fig. 2. Note that the $\tilde{\nu}_{gas}^{CO}$ has been subtracted in this figure. The band positioned around 2240 cm^{-1} is due to –NCO surface species [32]. Furthermore, the band at 2110 cm^{-1} has previously been assigned to CO adsorbed on platinum(II)oxide [23,24,26,27], while the band at 2082 cm^{-1} has been considered as CO adsorbed on partially oxidised platinum ($\tilde{\nu}_{lin}^{CO}(Pt^{\delta+})$) [26]. From these studies it is not evident that the band at 2110 cm^{-1} originates from CO on a platinum oxide with the stoichiometry Pt(II)O, it could also be related to CO on $Pt(IV)O_2$ since this is the thermally more stable oxide (Pt(II)O and $Pt(IV)O_2$ decompose at 598

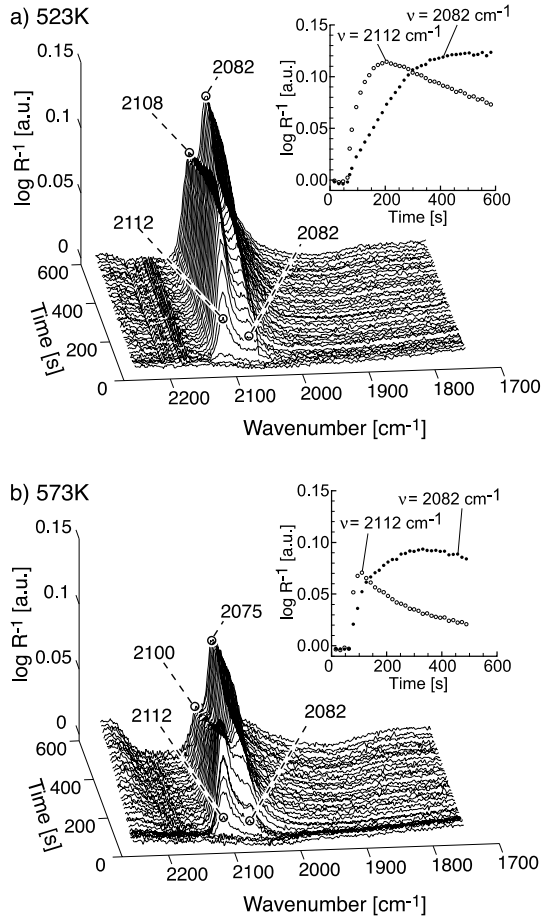

Fig. 2. Evolution of different IR bands in the interval 1750–2250 cm^{-1} during the switch from 0.0 to 1.0 vol% CO in Ar at $t = 60$ s for a 2.0% Pt/Al_2O_3 catalyst pretreated with 250 vol ppm NO_2 at 723 K for 10 min at (a) 523 and (b) 573 K. The inserts show the intensity at the wavenumbers 2082 ($\tilde{\nu}_{lin}^{CO}(Pt^{\delta+})$) and 2112 cm^{-1} ($\tilde{\nu}_{lin}^{CO}(Pt^{2+})$).

and 723 K, respectively [33]). However, the situation may be very different for supported Pt particles. It has been shown for Pt/Al_2O_3 catalysts, with similar Pt loading and dispersion as ours, that Pt(II)O is probably the more stable oxide form [34]. We will therefore refer to this band as CO on Pt(II)O or $\tilde{\nu}_{lin}^{CO}(Pt^{2+})$ in agreement with previous IR studies [23,24,26,27]. Fig. 2a shows that for 523 K the $\tilde{\nu}_{lin}^{CO}(Pt^{2+})$ band intensity passes through a maximum at $t = 204$ s while the intensity of the $\tilde{\nu}_{lin}^{CO}(Pt^{\delta+})$ increases continuously during the CO adsorption. However, at 573 K (cf. Fig. 2b) both bands pass through (different) maximum intensities. This occurs at $t = 110$ s for the $\tilde{\nu}_{lin}^{CO}(Pt^{2+})$ band and at $t = 340$ s for $\tilde{\nu}_{lin}^{CO}(Pt^{\delta+})$. As can be seen in Fig. 2, the $\tilde{\nu}_{lin}^{CO}(Pt^{2+})$ is red-shifted from 2112 to 2108 cm^{-1} at 523 K and from 2112 to 2100 cm^{-1} at 573 K during the CO adsorption. For the $\tilde{\nu}_{lin}^{CO}(Pt^{\delta+})$ band a red-shift can only be observed at 573 K starting at 2082 shifting to 2075 cm^{-1}.

In both the IR1 and the IR2-3 (not shown) experiments and the CO control experiment at 573 K on a NO_2-oxidised catalyst, a shift of $\tilde{\nu}_{lin}^{CO}$ band is observed. As will be discussed in more detail below, this red-shift cannot be ac-

counted for by CO–CO lateral interactions or impurities such as H_2O [30]. Instead it is natural to assign the red-shift to the presence of two bands: one band at higher wavenumber, which is weaker and disappears during the reduction phase, associated with CO adsorption on partially oxidised Pt, $\tilde{\nu}_{\text{lin}}^{\text{CO}}(\text{Pt}^{\delta+})$, and another (more intense) band, which is the conventional linearly bonded CO on metallic Pt, $\tilde{\nu}_{\text{lin}}^{\text{CO}}(\text{Pt}^0)$ or $\tilde{\nu}_{\text{lin}}^{\text{CO}}(\text{Pt})$ to conform to the conventional nomenclature, that grows during the reduction phase. To facilitate the analysis of these bands the $\tilde{\nu}_{\text{lin}}^{\text{CO}}$ bands were deconvoluted. The deconvolution procedure was performed using a non-linear, least-square fitting routine to Gaussian peaks wherein first the contribution from gas-phase CO was subtracted followed by subtraction of the spectrum for the reduced catalyst and one Gaussian. Due to the strong asymmetry of the $\tilde{\nu}_{\text{lin}}^{\text{CO}}(\text{Pt}^0)$ band, the average of the 10 spectra recorded during the reduction phase at $t = 598$–600 s was used to represent CO on the reduced catalyst. The Gaussian then represents linear bonded CO on partially oxidised Pt, which we denote $\tilde{\nu}_{\text{lin}}^{\text{CO}}(\text{Pt}^{\delta+})$. Both the height and the width of the Gaussian band were free to vary in all spectra while the band position was allowed only to vary between the different experiments (at 523–623 K). The fitted positions of $\tilde{\nu}_{\text{lin}}^{\text{CO}}(\text{Pt}^{\delta+})$ are summarised in Table 2.

The mass spectrometry data, recorded simultaneously with the FTIR data, are presented in Fig. 3. The top panels show the time evolution of the m/e 28, 32 and 44 signals while the bottom panels show the integrated $\tilde{\nu}_{\text{lin}}^{\text{CO}}$ and $\tilde{\nu}_{\text{br}}^{\text{CO}}$ bands for the temperatures 523, 573 and 623 K. The vertical (thin) lines represent different characteristic periods which will be explained below. In the following, the experiment at 523 K will be described carefully, while for the remaining temperatures only the main differences from this experiment will be pointed out in detail. In Fig. 3a it is seen that the reduction phase is initiated by turning off the O_2 supply at $t = 60$ s for a 300-s period. The O_2 switch is clearly seen as a decreased intensity of the m/e 32 signal. The decrease of the m/e 44 signal together with the increase of the m/e 28 signal indicates an extinction of the CO oxidation reaction. The m/e 28, 32 and 44 signals reach new stationary levels in about 70 s after turning off the O_2 supply. During the reduction phase a continuous increase of the $\tilde{\nu}_{\text{lin}}^{\text{CO}}(\text{Pt})$ and $\tilde{\nu}_{\text{br}}^{\text{CO}}$ band intensities is seen. Both bands increase rather quickly for the first 60 s and then somewhat more slowly during the remaining 240 s. Contrary to this, the intensity of $\tilde{\nu}_{\text{lin}}^{\text{CO}}(\text{Pt}^{\delta+})$ increases rapidly reaching a *maximum* value at $t = 90$ s, and then decays and disappears for the next 270 s. At $t = 360$ s, the O_2 supply is turned on again (oxidation phase) which can be seen as an increase of the m/e 32 signal. The onset of the CO oxidation is indicated by the decrease of the m/e 28 signal and the increase of the m/e 44 signal. The figure shows that the $\tilde{\nu}_{\text{lin}}^{\text{CO}}(\text{Pt})$ and $\tilde{\nu}_{\text{br}}^{\text{CO}}$ bands decrease and disappear immediately after the O_2 switch. No further changes are seen for the remaining time of the experiment.

In Fig. 3 it is clearly seen that the IR band intensity versus time depends on the temperature. After turning off

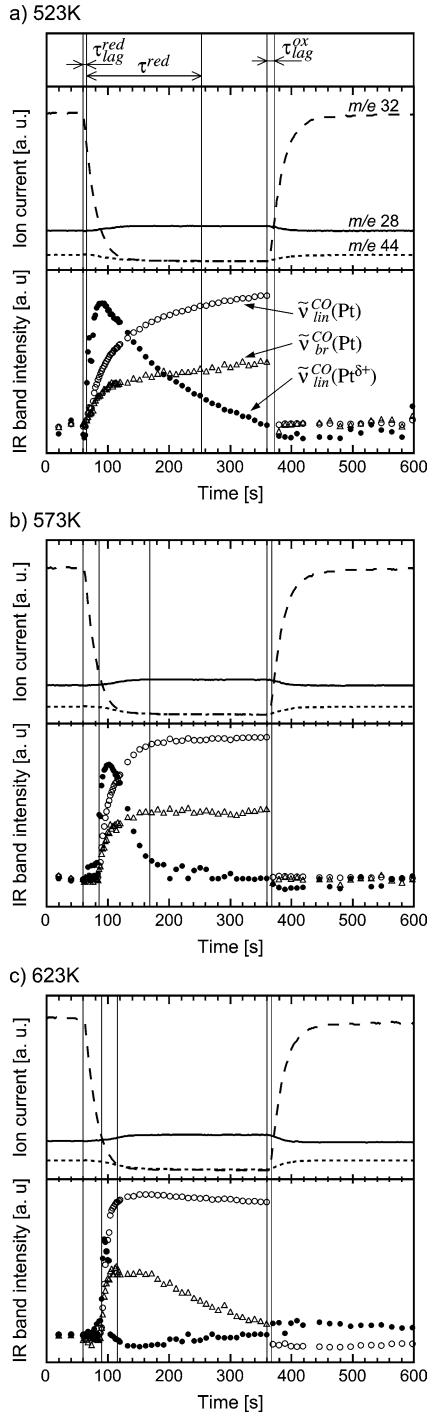

Fig. 3. Measured MS ion currents (m/e 28, 32, and 44) for the product stream (top panels) and integrated IR band intensities (bottom panels) for $\tilde{\nu}_{\text{lin}}^{\text{CO}}(\text{Pt})$, $\tilde{\nu}_{\text{br}}^{\text{CO}}(\text{Pt})$, and $\tilde{\nu}_{\text{lin}}^{\text{CO}}(\text{Pt}^{\delta+})$ for a 2.0% $\text{Pt/Al}_2\text{O}_3$ catalyst exposed to 1.0 vol% CO in Ar while switching the O_2 concentration from 5.0 to 0.0 vol% at $t = 60$ s (reduction phase) and then back to 5.0 vol% at $t = 360$ s (oxidation phase) at (a) 523, (b) 573, and (c) 623 K. The vertical (thin) lines represent the time lags for reduction and oxidation ($\tau_{\text{lag}}^{\text{red}}$ and $\tau_{\text{lag}}^{\text{ox}}$) and the reduction time (τ^{red}).

the O_2 supply at $t = 60$ s (reduction phase), the $\tilde{\nu}_{\text{lin}}^{\text{CO}}(\text{Pt})$, $\tilde{\nu}_{\text{lin}}^{\text{CO}}(\text{Pt}^{\delta+})$, and $\tilde{\nu}_{\text{br}}^{\text{CO}}$ bands start to increase. The initial slope for the $\tilde{\nu}_{\text{lin}}^{\text{CO}}(\text{Pt})$ and $\tilde{\nu}_{\text{br}}^{\text{CO}}$ intensities increases with increas-

Table 3
Summary of time constants for the $\tilde{\nu}_{lin}^{CO}$ band intensity for the reduction (τ_{lag}^{red} and τ^{red}) and the oxidation (τ_{lag}^{ox} and τ^{ox}) of a 2% Pt/Al_2O_3 catalyst at 523–623 K

Temperature (K)	τ_{lag}^{red} (s)	τ^{red} (s)	τ_{lag}^{ox} (s)	τ^{ox} (s)
523	5	188	12	0.5
548	17	163	7	0.5
573	26	83	8	0.5
598	28	55	8	0.5
623	30	25	7	0.7

ing temperature, while for $\tilde{\nu}_{lin}^{CO}(Pt^{\delta+})$ the slope is more or less constant at all temperatures. Furthermore, the bands for $\tilde{\nu}_{lin}^{CO}(Pt)$ and $\tilde{\nu}_{br}^{CO}$ increase monotonically toward stationary values which are reached more rapidly the higher the temperature. The $\tilde{\nu}_{lin}^{CO}(Pt^{\delta+})$ band intensity reaches a maximum similar to that previously described but the maximum is passed more rapidly the higher the temperature and also drops more rapidly with increasing temperature. At 623 K decomposition of unstable carbonates leads to negative band intensities (since the reaction mixture was used as IR reference) at low wavenumbers, which also affects the $\tilde{\nu}_{br}^{CO}$ band, as can be seen in Fig. 3c.

As already noted, the $\tilde{\nu}_{lin}^{CO}$ band appears with an initial time lag relative the gas switch. This is referred to as the reduction time lag (τ_{lag}^{red}). As can be noted in Fig. 1 and clearly in Fig. 3 and Table 3, τ_{lag}^{red} increases with increasing temperature. At 523 K τ_{lag}^{red} is about 5 s, while about 30 s at 623 K. Note that under the prevailing conditions, the time lag between the four-port switching valve and the reactor cell is about 2 s. Moreover, considering the reactor chamber as an ideal continuously stirred tank reactor, the average residence time is about 5 s and the time to reach a 90% response is about 10 s. Furthermore, as described above, a red shift of the $\tilde{\nu}_{lin}^{CO}$ band could be observed for all temperatures during the reduction phase. This period with shifting $\tilde{\nu}_{lin}^{CO}$ is referred to as the reduction time (τ^{red}) and is defined as the length of the period between the first appearance of the $\tilde{\nu}_{lin}^{CO}$ band and when this band reaches a stationary wavenumber. As is evident from Fig. 3 and Table 3, τ^{red} decreases with increasing temperature, from about 188 s at 523 K to about 25 s at 623 K (IR1). At $t = 360$ s the O_2 supply, 5.0%, is turned on again (oxidation phase). All IR bands vanish abruptly with a short time lag, which here is referred to as the oxidation time lag (τ_{lag}^{ox}) and defined in analogy with τ_{lag}^{red}. No clear trend in the τ_{lag}^{ox} with increasing temperature can be observed, see Table 3. The time then for the $\tilde{\nu}_{lin}^{CO}$ to completely vanish is referred to as the oxidation time (τ^{ox}). The τ^{ox} is about 0.5 s for all temperatures in the IR1 series.

Analogous to the IR1 series, the τ_{lag}^{red} increases with increasing temperature for the IR2 experiments. In this case τ_{lag}^{red} is about 40 s longer, varying from 42 s at 523 K to 68 s at 623 K, which is due to the generally lower CO/O_2 ratio, where 1000 ppm CO was used instead of 1.0% CO (IR1). Accordingly, the high CO/O_2 ratio in the IR3 series, where 1.0% O_2 was used instead of 5.0%, leads to shorter τ_{lag}^{red} compared to the IR1 series. Contrary to both the IR1 and the IR2 series, no trend of increasing τ_{lag}^{red} with increasing temperature is observed for the IR3 series. Instead, τ_{lag}^{red} is about 8 s at all temperatures between 548 and 623 K (an oscillating reaction rate was observed in the high reactive state at 523 K and data for this experiment are therefore not considered), which is of the same order as the typical response time for changing gas composition in the reactor cell. This is probably explained by that even in the high reactive state the reaction proceeds close to the critical CO/O_2 ratio at which the transition between the high and low the reaction occurs rate branch. Turning off the O_2 supply, the critical CO/O_2 ratio is reached and passed very rapidly at all temperatures and hence the different τ_{lag}^{red} are here experimentally indistinguishable. In contrast, τ^{red} decreases with increasing temperature for both the IR2 and the IR3 series similar to the IR1 series. Compared to the IR1 experiments, τ^{red} is generally longer for the IR2 experiments while it is shorter for the IR3 experiments. Considering τ_{lag}^{ox}, the IR2 experiments resembles the IR1 experiments exhibiting no trend with changing temperature. Similarly to the arguments above, this may be explained by the fact that the critical CO/O_2 ratio is reached and passed very rapidly when the O_2 concentration is changed stepwise from 0.0 to 5.0%, making the different τ_{lag}^{ox} experimentally indistinguishable. Again the IR3 experiments exhibit somewhat different characteristics, which we attribute to a different gas mixing ratio and different location of a critical CO/O_2 ratio. Contrary to the IR1 series both the IR2 and the 3 series show a slightly increasing τ^{ox} with increasing temperature. This can again be related to different gas mixing ratio and different location of the critical CO/O_2 ratio but also to CO disproportionation during the periods with high CO coverage [31]. This is, however, of minor importance since it is the initial CO adsorption that will be discussed here. It should also be noted that the τ_{lag}^{red} in the CO adsorption control experiments on NO_2-oxidised samples are 2 and 4 s at 523 and 573 K, respectively, which simply is the time lag for introducing new gas to the reactor cell.

3.2. *In situ XANES*

Figs. 4a and 4b show a few selected Pt L_{III} XANES spectra (normalised absorbance versus photon energy) obtained during the reduction phase at 523 and 623 K, respectively. As can be seen the white-line intensity, at about 11580 eV, is generally higher at the lower temperature. The white-line intensity then decreases as a function of time on stream, indicating a reduction of the oxidation state for Pt. Moreover, a shift of the curves toward higher photon energies is observed for the same period. This shift is used as a measure of the Pt L_{III} binding energy (see also Experimental) below.

The results from the XANES experiments during the reduction and subsequent oxidation phases performed at 523

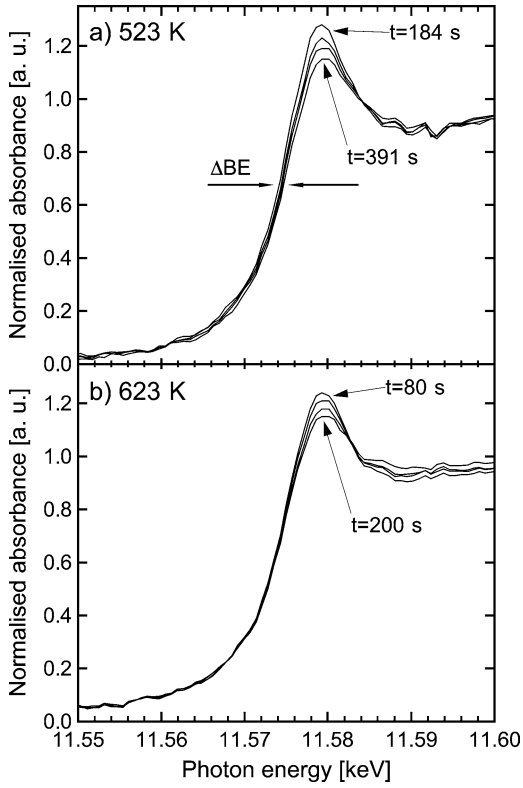

Fig. 4. Pt L_{III} XANES spectra for a Pt/Al_2O_3 catalyst exposed to 1.0 vol% CO in Ar while switching the O_2 concentration from 5.0 to 0.0 vol% (reduction phase) at (a) $t = 184$ s at 523 K and (b) $t = 80$ s at 623 K.

and 623 K are shown in Figs. 5 and 6, respectively. The top panels display the measured m/e signals while the bottom panels show the change in Pt L_{III} binding energy (ΔBE) as a function of time for the Pt/Al_2O_3 sample.

In Fig. 5, the reduction phase is initiated by turning off the O_2 supply at $t = 120$ s. This can be recognized in the intensity of the m/e 32 signal, dropping fast for about 15 s and then decaying more slowly. The intensity of the m/e 28 signal increases rapidly to a new stationary level while the intensity of the m/e 44 signal decreases, first quickly and then more slowly for the next 280 s, during this reduction phase. For the same period the binding energy increases monotonically to a new stationary level, about 0.6 eV above the initial binding energy of 11573.2 eV. The τ_{lag}^{red}, the time between the gas switch and the first observable variation of the ΔBE, is less than 25 s and the τ^{red}, here defined as the time between the first observable change of ΔBE and the stationary ΔBE, is about 200 s. The oxidation phase is initiated by switching back to 5.0% O_2 at $t = 370$ s. An overshoot in the m/e 32 signal before it stabilises at a higher level is seen. The intensity of the m/e 28 signal drops and is somewhat unstable before it levels out on a stationary level. This is simply due to the fact that the gas switching was performed by the use of the MFC. A rapid increase of the m/e 44 signal to a new level is seen during this phase. The binding energy decreases rather quickly with 0.4 eV. The τ_{lag}^{ox} is less than 30 s and the τ^{ox} is less than 50 s.

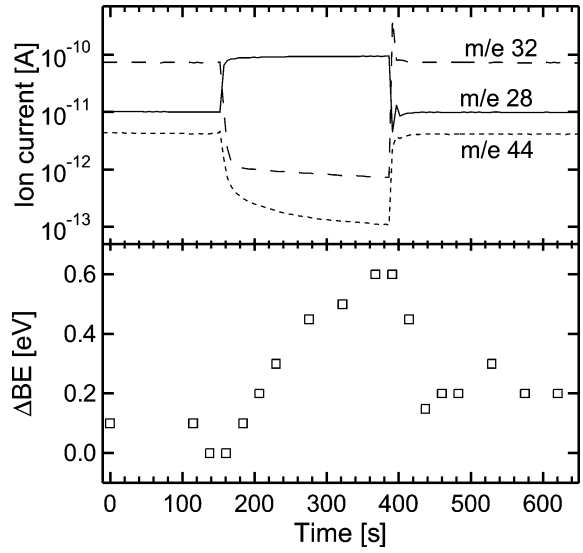

Fig. 5. Measured MS ion currents (m/e 28, 32, 44) for the product stream (top panel) and change in the Pt L_{III} binding energy (ΔBE) from 11572.2 eV (bottom panel) for a 2.0%Pt/Al_2O_3 catalyst exposed to 1.0 vol% CO in Ar while switching the O_2 concentration from 5.0 to 0.0 vol% at $t = 120$ s (reduction phase) and then back to 5.0 vol% at $t = 400$ s at 523 K.

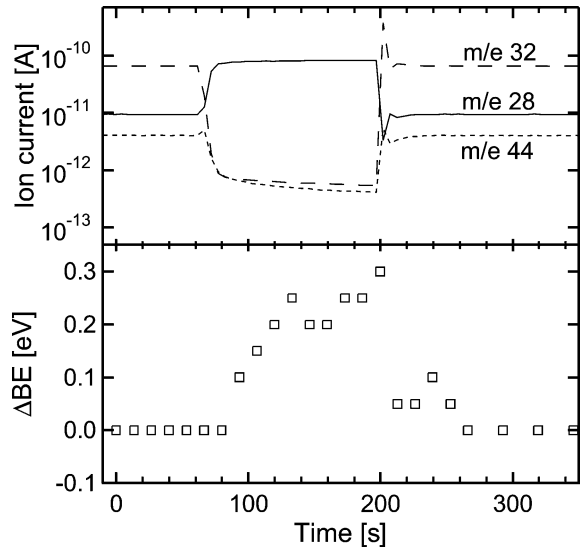

Fig. 6. Measured MS ion currents (m/e 28, 32, 44) for the product stream (top panel) and change in the Pt L_{III} binding energy (ΔBE) from 11,573.5 eV (bottom panel) for a 2.0% Pt/Al_2O_3 catalyst exposed to 1.0 vol% CO in Ar while switching the O_2 concentration from 5.0 to 0.0 vol% at $t = 60$ s (reduction phase) and then back to 5.0 vol% at $t = 190$ s at 623 K.

In the case of 623 K, Fig. 6, the reduction phase starts when the O_2 supply is turned off at $t = 60$ s (the intensity of the m/e 32 signal drops) which is seen as a decrease and a corresponding increase of the m/e 44 and m/e 28 signals, respectively. The binding energy (with an τ_{lag}^{red} less than 25 s) increases with about 0.3 eV from the initial value of 11,573.5 eV and reaches a stationary level within about 50 s. The oxidation phase is initiated by turning on the O_2 supply

again (increasing intensity of the m/e 32 signal) as seen as a drop in the m/e 28 signal, which is somewhat unstable before it levels a stationary intensity. During this period a rapid increase of the m/e 44 signal to a new level is seen. The binding energy decreases by 0.3 eV rather quickly (with an $\tau_{\text{lag}}^{\text{ox}}$ less than 20 s) and reaches the initial level in less than 15 s.

4. Discussion

This study shows that FTIR spectroscopy can be used to follow the change in oxidation state of a supported platinum catalyst in situ by measuring the vibrational frequency of adsorbed CO. Here CO is used as a probe molecule while it simultaneously acts as a reducing agent. In this section, we consider the FTIR data in detail and make comparisons with corresponding in situ XANES data to validate the FTIR interpretations. Based on the experimental data we are able to deduce a mechanistic interpretation of the reduction process of the Pt/Al_2O_3 catalyst. Finally, we make some reflections on the influence of diffusion limitations (both external and internal) on the reaction rate for the FTIR experiments.

In all CO oxidation experiments in this study, the reaction initially proceeds in the high reactive state with the corresponding low CO coverage as evidenced by the FTIR data presented in Figs. 1 and 3. At $t = 60$ s, the O_2 supply is turned off (reduction phase commences) and the O_2 pressure in the reactor chamber starts to decline. It is evident that the CO coverage gradually builds up after an initial time lag ($\tau_{\text{lag}}^{\text{red}}$) which depends on temperature. It is also evident that the $\tilde{\nu}_{\text{lin}}^{\text{CO}}$ band is red shifted about 15 cm^{-1} in all experiments performed at 523–623 K (cf. Fig. 1) during the initial CO adsorption. As will be further discussed below the $\tau_{\text{lag}}^{\text{red}}$ and its temperature dependence may be interpreted according to the conventional LH reaction scheme, i.e., steps (1)–(3). In contrast, the gradual increase of the CO coverage and the red-shift of the $\tilde{\nu}_{\text{lin}}^{\text{CO}}$ band cannot be explained with the LH reaction scheme. The latter is in fact opposite to the expected scenario for metallic Pt where instead a small blue-shift of about 5 cm^{-1} is anticipated when CO starts to adsorb and the coverage increases [26,30]. This blue-shift is mainly due to increasing repulsive CO–CO adsorbate interactions and has been observed to be enhanced at high CO pressure when CO is forced to occupy also unfavorable Pt sites, i.e., not the energetically favorable on-top sites [30,35]. Experimentally, repulsive CO–CO adsorbate interactions can also be seen as a decrease in the heat of adsorption as the surface coverage increases [36]. Furthermore in our experiments, possible interactions with coadsorbates such as water, which is known to red-shift the $\tilde{\nu}_{\text{lin}}^{\text{CO}}$ band [30], can be ruled out due to careful drying of the sample before measuring and the use of high-purity gases. A negligible influence of water is further emphasised by the fact that we study rather high temperatures and that the magnitude of the red-shift does not decrease as the temperature is increased, which probably would have been the case if water were present on the surface (a shift of the water adsorption–desorption equilibria toward desorption). Hence, the red-shift of the $\tilde{\nu}_{\text{lin}}^{\text{CO}}$ band observed in our measurements needs another explanation which motivated us above to resolve the observed $\tilde{\nu}_{\text{lin}}^{\text{CO}}$ band into two different bands, viz. $\tilde{\nu}_{\text{lin}}^{\text{CO}}(\text{Pt}^0)$ and $\tilde{\nu}_{\text{lin}}^{\text{CO}}(\text{Pt}^{\delta+})$. The red-shift is thus attributed to an initial CO adsorption on an oxide phase of Pt. Since the wavenumber for this band is positioned between the $\tilde{\nu}_{\text{lin}}^{\text{CO}}(\text{Pt}^0)$ and the $\tilde{\nu}_{\text{lin}}^{\text{CO}}(\text{Pt}^{2+})$ bands we attribute this band to CO linearly bonded to $\text{Pt}^{\delta+}$. The occurrence of an intensity maximum for the $\tilde{\nu}_{\text{lin}}^{\text{CO}}(\text{Pt}^{\delta+})$ band in Fig. 3 is thus due to CO first being adsorbed on these sites (increasing intensity) before the reduction starts and the number of $\text{Pt}^{\delta+}$ sites decreases (decreasing intensity). As the oxidised Pt sites are being reduced, the number of available sites for CO adsorption on metallic Pt increases, leading to a continuously increasing intensity of the $\tilde{\nu}_{\text{lin}}^{\text{CO}}(\text{Pt})$ and $\tilde{\nu}_{\text{br}}^{\text{CO}}$ bands. The XANES experiments also indicate a similar reduction process. The change in binding energy, which is small, about 0.5 eV, occurs on the same time scale as the $\tilde{\nu}_{\text{lin}}^{\text{CO}}$ band changes, i.e., τ^{red}. Since the XANES signal is averaged over the entire illuminated catalyst tablet volume, including bulk Pt atoms in Pt clusters and Pt atoms coordinated with the support material, it may be difficult to deduce absolute shifts from XANES relevant for the surface Pt atoms involved in the catalytic cycle. However, XANES has previously been shown to be useful for correlating structure to catalytic activity also for supported catalysts [37,38]. Given that the red-shift of $\tilde{\nu}_{\text{lin}}^{\text{CO}}$ is associated with (partially) oxidised Pt, we may explain the observed trends in τ^{red} and $\tau_{\text{lag}}^{\text{red}}$ as follows.

If τ^{red} is associated with CO being successively adsorbed on sites coordinated with $\text{Pt}^{\delta+}$ as the oxide is reduced by CO, then τ^{red} is a measure of the rate of step (5). This is an activated process, which results in the observed decrease of τ^{red} as the temperature is increased. Assuming that the reduction rate is inversely proportional to the τ^{red}, an Arrhenius plot of $\ln(1/\tau^{\text{red}})$ versus $1/T$ gives an estimate of the activation energy ($E_{\text{a}}^{\text{red}}$) for the reduction process. Fig. 7 displays the Arrhenius plot based on FTIR data from the IR1 series together with the corresponding XANES data. The XANES experiments should give the same result for the $E_{\text{a}}^{\text{red}}$, although it may be located at a different level on the ordinate. According to this procedure the apparent $E_{\text{a}}^{\text{red}}$ is 54.9 kJ/mol. Note, however, that we measure the decay of $\tilde{\nu}_{\text{lin}}^{\text{CO}}(\text{Pt}^{\delta+})$ species, i.e., the number of $\text{Pt}^{\delta+}$ sites, which not necessarily is proportional to the oxide decomposition rate, which in principle is the sum of step (4) (backward) and (5). It is known that platinum oxides are thermodynamically unstable at the highest temperature in this study. These oxides decompose between 623 and 723 K (depending on the oxide stoichiometry) [33]. Considering for example step (4), i.e., that a thermal decomposition of the oxide should be considered at the highest temperatures, we may omit these

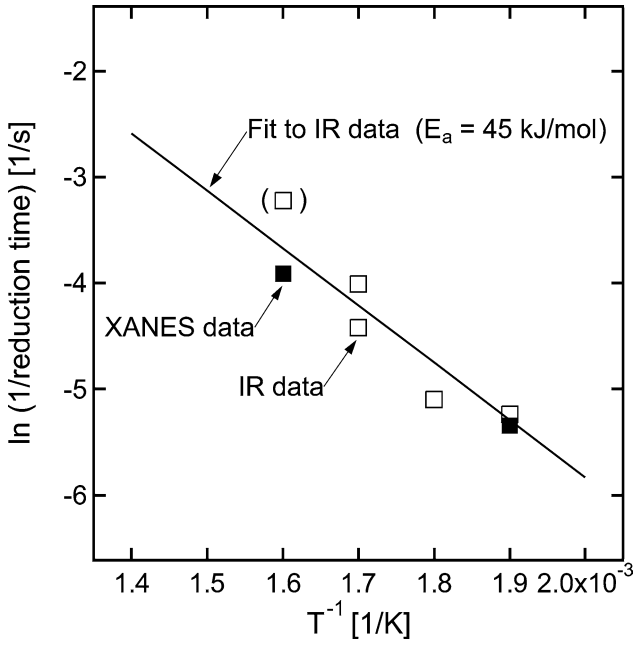

Fig. 7. Arrhenius plot of IR and XANES data for the reduction process of a 2%Pt/Al_2O_3 catalyst exposed to 1.0 vol% CO while switching the O_2 concentration from 5.0 to 0.0 vol%. The fit is based on the IR data with the highest temperature of 623 K excluded.

data points and arrive at a value of the activation energy of 45.1 kJ/mol, which is close to the previously reported value of 44 kJ/mol [39].

The variation of τ_{lag}^{red} in Table 3 is also consistent with a Pt oxidation and reduction mechanism. First, we note that the magnitude and variation of τ_{lag}^{red} cannot be explained by the time to evacuate the reactor chamber from O_2 (cf. Table 3) or by diffusion limitations (see below). The CO adsorption control measurements performed on the reduced and oxidised catalyst, respectively, all exhibit similar lag times for all temperatures (of the order of 5 s after the gas switch). Moreover, the reaction chamber is drained of O_2 almost equally fast for all temperatures (the O_2 concentration is about the same in all experiments since the CO conversion is low, about 15–20%). In a simple picture an increase of τ_{lag}^{red} with temperature can be interpreted as a shift of the CO adsorption–desorption equilibrium, which of course favors CO adsorption at low temperature and is the same result as anticipated from the conventional LH model. However, according to the interpretation of $\tilde{\nu}_{lin}^{CO}$ above, τ_{lag}^{red} is related to adsorption of CO on $Pt^{\delta+}$ sites prior to reduction commences. The latter can enhance the variations of τ_{lag}^{red}. If the rate of CO desorption is of the same order or faster than a slow $CO + O_{ox}$ reaction step (in the conventional LH scheme the $CO + O_{ads}$ reaction rate is much faster than the rate of CO desorption) [10,40], the CO coverage can build up faster at lower temperature on the oxide surface than on the metallic Pt surface. In the opposite case, if the $CO + O_{ox}$ is faster than the $CO + O_{ads}$ LH step Eq. (3) [41], then the variation in τ_{lag}^{red} is anticipated to be reduced compared to the variation induced by the shift of the CO adsorption–desorption equilibrium.

As discussed above we cannot unambiguously resolve CO bonded to the oxide between 2100 and 2130 cm^{-1} in the IR1-3 experiments (Fig. 1). This is either due to the overlapping gas phase CO bands, or a low coverage (due to weak bonding to such O sites). However, the fact that $\tilde{\nu}_{lin}^{CO}(Pt^{2+})$ bands around 2110 cm^{-1} indeed can be observed for the same catalyst preoxidised with NO_2 (strongly oxidised) shows that such species exist under our experimental conditions. Therefore, we conclude that the weaker IR absorption in the $\tilde{\nu}_{lin}^{CO}(Pt^{2+})$ region in the IR1-3 experiments is due to CO adsorbed on Pt oxide which only exists in low amounts. Moreover, since we found an IR band positioned between 2054 and 2066 cm^{-1} (cf. Table 2), depending on temperature, which we associated with $\tilde{\nu}_{lin}^{CO}(Pt^{\delta+})$, we conclude that the surface is instead partially oxidised. We also note that our results are consistent with a reaction scheme whereby CO adsorbs and binds (weakly) on the stoichiometric oxides (PtO or PtO_2) and reacts with these O atoms, possibly creating vacancies opening for the reaction scheme (1)–(5) above.

The combined FTIR and XANES results above provide a consistent picture of the extinction process on supported Pt catalysts and explicitly highlight the influence of Pt oxide on the catalytic activity. It is clearly shown that the transition from an O to a CO covered surface, the “extinction” process, occurs on a much longer time scale than the reverse transition from a CO to an O covered surface, the “ignition” process. This hysteresis is in sharp contrast to what the conventional LH reaction model predicts, where instead the two transitions occur equally fast (of course at different CO/O_2 ratios). We can attribute this hysteresis as being due to Pt oxide, which builds up in the high reactive state (oxygen rich surface), and changes the adsorption kinetics. Our FTIR data obtained during the extinction process show the existence of CO adsorption sites coordinated with partially oxidised Pt. It should be noted that CO adsorption sites coordinated with more strongly oxidised Pt have only been observed for NO_2-treated catalysts. In agreement with previous studies, the results presented here thus suggest that a Pt oxidation and reduction mechanism, i.e., steps (4) and (5), should accompany the conventional LH reaction scheme in order to describe the CO oxidation over Pt/Al_2O_3 catalysts under transient conditions. Furthermore, the results indicate that during the extinction the partially oxidised surface is reduced by chemisorbed CO, which should be explicitly accounted for in the modelling of the reaction mechanism, and should not be approximated with an Eley–Rideal step ($CO_{gas} + O_{ox} \rightarrow (CO_2)_{gas}$).

We close this discussion with some reflections on possible diffusion limitations affecting the reaction rate in our FTIR experiments. It is well known that diffusion limitations may falsify the interpretations of kinetics, especially in transient analysis which always includes such phenomena. Since the reactor cell with the catalyst can be regarded

as a small packed-bed reactor with porous alumina particles, both external (film transport) and internal (pore transport) diffusion processes must be considered. We start by investigating the situation for the high reactive state during stationary conditions, $t < 1$ min, for the IR1 series. The influence of external diffusion on the reaction rate can easily be estimated by calculating the concentration difference of CO over the gas film (ΔC_{CO}) and compare this value with the concentration of CO in the gas bulk, as outlined in Appendix A. As can be seen, ΔC_{CO} is in the order of 10^{-4} mol/m^3 which is negligible compared to the bulk gas concentration of about 0.2 mol/m^3. This implies the absence of external diffusion limitations. The influence of internal diffusion on the reaction rate can then be estimated by calculating the Weisz modulus and use the Weisz–Prater criterion (cf. Appendix B). As can be seen this method predicts no internal diffusion limitations. Furthermore, as outlined in Appendix C, the impingement rate is about 6 orders of magnitude higher than the observed reaction rate. This is in sharp contrast to the conventional LH model for which the reaction rate on the high reaction rate branch is much faster than the impingement rate. This suggests again that the surface is oxidised where the low CO coverage is due to weak binding on platinum oxides. Finally, some words need to be said about diffusion limitations during transient conditions (the O_2 switches). In the transient regime, diffusion limitations will be present for some periods and thereby influence the kinetics to some extent. In our case, at some point after the oxygen supply has been turned off, CO starts to adsorb on the platinum sites. The time to saturate the adsorption sites, i.e., active sites, in the catalyst with CO depends on e.g., the internal diffusion (transport rate) and the number of sites (CO accumulation). The time constant for accumulation of 1 ML CO (extinction) is roughly a couple of seconds (cf. Appendix D) while a somewhat shorter time constant is anticipated for the ignition. Hence, the observed changes of, e.g., the CO coverage, during the extinction origins from kinetic (structural) effects of the catalyst, rather than mass transport since the former has been observed to occur for minutes.

5. Conclusions

We have presented experimental results for the oxidation of CO over Pt/Al_2O_3 catalysts. In particular, we have investigated the extinction process of the reaction over a catalyst operating in an O_2-rich reaction mixture at atmospheric pressure. Detailed data for the initial reduction process by CO of a partially oxidised Pt surface are presented, including the CO coverage and Pt oxidation state. The results, which are at variance with the conventional three-step LH reaction scheme, show that a Pt oxidation and reduction mechanism must be invoked in the LH reaction scheme to accurately describe the extinction process. Specifically, this is supported by the following findings: (i) The transition from an O to a CO covered surface occurs much slower than the reverse transition from a CO to an O covered surface. This can be explained by neither external or internal diffusion limitations. In the conventional LH model both transitions occur equally rapid as the critical CO/O_2 ratio is reached. (ii) The transition from an O to a CO covered surface is clearly temperature dependent, the reduction time (τ^{red}) decreases with increasing temperature, which is not anticipated by the conventional LH model. (iii) The $\tilde{\nu}_{lin}^{CO}$ band is red-shifted during the reduction period, which cannot be explained by reported trends for CO adsorption vs coverage on a metallic surface. (iv) The XANES data show that Pt reduction occurs on the same time scale as the $\tilde{\nu}_{lin}^{CO}$ frequency shifts (τ^{red}) during the extinction process, which suggests an intimate coupling between the activity and the oxidation state of platinum. (v) The temperature dependent decay of the FTIR band associated with PtO_x ($\tilde{\nu}_{lin}^{CO}(Pt^{\delta+})$) yields an activation energy for Pt oxide reduction (decomposition) of about 50 kJ/mol in good agreement with previous reports for Pt oxide decomposition, and finally, (vi) FTIR data suggest that during the extinction the partially oxidised platinum surface is reduced by chemisorbed CO which should be explicitly accounted for in the modeling of the reaction mechanism.

Acknowledgments

This work has been performed within the Competence Centre for Catalysis, which is hosted by Chalmers University of Technology and financially supported by the Swedish Energy Agency and the member companies: AB Volvo, Johnson Matthey-CSD, Saab Automobile Powertrain AB, Perstorp AB, AVL-MTC AB, Akzo Nobel Catalysts BV and the Swedish Space Agency. The authors thank the European Synchrotron Radiation Facility (ESRF) in Grenoble, France, for granting the XANES beam time. Dr. Sakura Pascarelli at beamline ID24 is gratefully thanked for her assistance with the XANES experiments. Prof. Vladimir P. Zhdanov is thanked for valuable discussions.

Appendix A. Influence of external diffusion limitations

The influence of external diffusion limitations on the reaction rate can be estimated by calculating the concentration difference of CO over the gas film (ΔC_{CO}). First we note that the observed reaction rate approximately is

$$r_{obs} = q\frac{p_{CO}}{RT}\frac{X}{W}, \tag{A.1}$$

where q is the volumetric flow rate at room temperature (2.5×10^{-6} m^3/s), p_{CO} is the partial pressure of CO (10^3 Pa), R is the molar gas constant (8.31 J/(mol K), T is temperature (300 K), X is the CO conversion (0.2), and W is the amount of catalyst (3×10^{-5} kg). Substituting the given values one obtains $r_{obs} = 6.7 \times 10^{-3}$ mol/(s kg$_{cat}$).

For a packed-bed reactor (with spherical catalyst pellets) under steady-state conditions, the reaction rate is coupled to

the film transport by

$$r = S_m k_c \Delta C_{CO}, \tag{A.2}$$

where $S_m = 6/d_p\rho_p$ is the external surface area of the pellet per mass of pellet and d_p and ρ_p are the pellet diameter and density, respectively. $k_c = \mathrm{Sh}D_{AB}/d_p$ is then the mass-transfer coefficient where Sh is the Sherwood number and D_{AB} the binary gas diffusivity. Solving for ΔC_{CO} gives

$$\Delta C_{CO} = \frac{r d_p^2 \rho_p}{6\mathrm{Sh}D_{AB}}. \tag{A.3}$$

Substituting r_{obs} for r and assuming a reasonable low value for the Sherwood number (Sh = 1.5) will produce an estimate of the largest concentration gradient. Using $d_p = 150 \times 10^{-6}$ m^2, $\rho_p = 1.5 \times 10^3$ kg/m^3, $D_{AB} = 6.1 \times 10^{-5}$ m^2/s one arrives at $\Delta C_{CO} = 4.2 \times 10^{-4}$ mol/m^3 which is negligible compared to the concentration in the gas bulk, $C^b_{CO} = p_{CO}/(RT) = 0.19$ mol/m^3 at $T = 623$ K.

Appendix B. Influence of internal diffusion limitations—Weisz–Prater method

The influence of internal diffusion limitations in a porous catalyst can be estimated by calculating the Weisz modulus,

$$\Phi = \frac{r_v r_p^2}{C^s_{CO} D_{eff}}, \tag{B.1}$$

where r_v is the reaction rate per volume of catalyst, r_p is the pellet radius, C^s_{CO} is the CO concentration at the surface of the pellet, and D_{eff} is the effective diffusivity. The Weisz–Prater criterion can then be used; i.e., for an isothermal spherical catalyst pellet and a first-order reaction, $\Phi < 1$ implies a particle free from internal concentration gradients. This corresponds to a high efficiency factor, $\eta \geqslant 0.95$.

Since the external diffusion limitations are negligible (cf. Appendix A), the concentration at the surface of a catalyst particle is well approximated with the concentration in the gas bulk, hence,

$$\Phi = \frac{r_{obs}\rho_{cat} r_p^2}{C^b_{CO} D_{eff}}, \tag{B.2}$$

where $r_{obs} = 6.7 \times 10^{-3}$ mol/(s kg$_{cat}$), $\rho_p = 1.5 \times 10^3$ kg/m^3, $r_p = 75 \times 10^{-6}$ m^2, $C^p_{CO} = 0.19$ mol/m^3, and $D_{eff} = 3.8 \times 10^{-7}$ m^2/s gives $\Phi \approx 0.77 < 1$, indicating the absence of internal diffusion limitations.

Appendix C. Impingement rate versus reaction rate

Due to the absence of diffusion limitations it is easy to calculate the CO impingement rate according to

$$F = \frac{N_A a_s p_{CO}}{\sqrt{2\pi M RT}}, \tag{C.1}$$

where N_A is the Avogadro constant (6.022×10^{23} 1/mol), a_s is the area of a Pt site (8×10^{-20} m^2), M is the CO molecular weight (28×10^{-3} kg/mol). With $p_{CO} = 10^3$ Pa and $T = 623$ K one obtains $F = 1.6 \times 10^6$ molecules/(site s).

The observed reaction rate per site is

$$r_{obs} = q\frac{p_{CO}}{RT}\frac{X}{n_s}, \tag{C.2}$$

where n_s is the number of sites which is given by

$$n_s = W[\text{Pt loading}][\text{Pt dispersion}]/M_{Pt}, \tag{C.3}$$

where M_{Pt} is the Pt molecular weight (0.195 kg/mol). With Pt loading = 0.02, Pt dispersion = 0.22 the reaction rate is $r_{obs} = 0.3$ molecules/(site s), and the ratio between the impingement rate and the reaction rate is

$$\frac{F}{r_{obs}} = \frac{1.6 \times 10^6}{0.3} \approx 5 \times 10^6. \tag{C.4}$$

Appendix D. Internal diffusion limitations in the transient regime

In order to estimate the influence of diffusion limitations during the extinction process both reaction and diffusion should be considered. This is, however, not straightforward and instead one can perform a (rough) estimation of the time constant for adsorbing 1 ML of CO on the active sites, in analogy with the shrinking-core model (strong CO adsorption is assumed), viz.

$$\tau = \frac{r_p^2 \rho_{cat}[\text{Pt loading}][\text{Pt dispersion}]}{D_{eff} M_{Pt} C^b_{CO}}. \tag{D.1}$$

This gives $\tau = 2.6$ s. This is an underestimation since most probably 1 ML (at least) of oxygen has to be reacted away during the extinction. On the other hand there is already some CO present in the porous support since the conversion was only 0.2 (no diffusion limitations). Somewhat shorter response time is anticipated for the ignition process since this occurs for oxygen excess conditions (oxygen is already available in the alumina particle).

References

[1] I. Langmuir, Trans. Faraday Soc. 17 (1922) 672.
[2] R.M. Heck, R.J. Farrauto, Appl. Catal. A 221 (2001) 443.
[3] G. Ertl, T. Engel, Adv. Catal. 28 (1979) 1.
[4] G. Ertl, Adv. Catal. 37 (1990) 1.
[5] P.D. Nolan, B.R. Lutz, P.L. Tanaka, J.E. Davis, C.B. Mullins, J. Chem. Phys. 111 (8) (1999) 3696.
[6] A.N. Artsyukhovich, V.A. Ukraintsev, I. Harrison, Surf. Sci. 347 (1996) 303.
[7] C.-L. Kao, A. Carlsson, R.J. Madix, Surf. Sci. 497 (2002) 356.
[8] V.P. Zhdanov, B. Kasemo, Surf. Sci. Rep. 20 (1994) 111.

[9] M. Bär, Ch. Zülicke, M. Eiswirth, G. Ertl, J. Chem. Phys. 96 (1992) 8595.
[10] S. Johansson, L. Österlund, B. Kasemo, J. Catal. 201 (2001) 275.
[11] D.A. Frank-Kamenetskii, in: Diffusion and Heat Transfer in Chemical Kinetics, Plenum, New York, 1969, p. 487.
[12] P. Hugo, Ber. Bunsenges. Phys. Chem. 74 (1970) 121.
[13] B.C. Sales, J.E. Turner, M.B. Maple, Surf. Sci. 114 (1982) 381.
[14] C.D. Lund, C.M. Surko, M.B. Maple, S.Y. Yamamoto, Surf. Sci. 459 (2000) 413.
[15] A. von Oertzen, H.H. Rotermund, A.S. Mikhailov, G. Ertl, J. Phys. Chem. B 104 (2000) 3155.
[16] H.H. Rotermund, M. Pollmann, I.G. Kevrekidis, Chaos 12 (2002) 157.
[17] P.-A. Carlsson, M. Skoglundh, P. Thormählen, B. Andersson, Top. Catal. 30/31 (2004) 375.
[18] P.J.F. Harris, Int. Mat. Rev. 40 (1995) 97.
[19] V.P. Zhdanov, B. Kasemo, Appl. Surf. Sci. 74 (1994) 147.
[20] P. Lööf, B. Kasemo, S. Andersson, A. Frestad, J. Catal. 130 (1991) 181.
[21] L. Olsson, E. Fridell, J. Catal. 210 (2002) 340.
[22] M. Sanchez del Rio, R.J. Dejus, in: XOP: Recent Developments, vol. 2448, SPIE-Int. Soc. Opt. Engeneering, Bellingham,WA, 1998, p. 340.
[23] M. Primet, J.M. Basset, M.V. Mathieu, M. Prettre, J. Catal. 29 (1973) 213.
[24] N. Sheppard, T.T. Nguyen, Adv. Infr. Raman Spectrosc. 5 (1978) 67.
[25] D.M. Haaland, F.L. Williams, J. Catal. 76 (1982) 450.
[26] M. Primet, J. Catal. 88 (1984) 273.
[27] J.A. Andersson, C.H. Rochester, J. Chem. Soc. Faraday. Trans. 87 (1991) 1479.
[28] A. Bourane, O. Dulaurent, D. Bianchi, Langmuir 17 (2001) 5496.
[29] NIST Standard Reference Database Number 69, 2003.
[30] G. Rupprechter, T. Dellwig, H. Unterhalt, H.-J. Freund, J. Phys. Chem. B 105 (2001) 3797.
[31] P. Thormählen, M. Skoglundh, E. Fridell, B. Andersson, J. Catal. 188 (1999) 300.
[32] F. Acke, B. Westerberg, M. Skoglundh, J. Catal. 179 (1998) 528.
[33] D.R. Lide, in: CRC Handbook of Chemistry and Physics, 76th ed., CRC Press, New York, 1995, pp. 4–76.
[34] C.-B. Wang, C.-T. Yeh, J. Catal. 178 (1998) 450.
[35] E. Kruse Vestergaard, P. Thostrup, T. An, E. Lægsgaard, I. Stensgaard, B. Hammer, F. Besenbacher, Phys. Rev. Lett. 88 (25) (2002) 259601-1.
[36] W.A. Brown, R. Kose, D.A. King, Chem. Rev. 98 (1998) 797.
[37] D. Schmitt, H. Fuess, H. Klein, U. Neuhausen, E.S. Lox, Top. Catal. 16/17 (2001) 355.
[38] H. Yoshida, Y. Yazawa, N. Takagi, A. Satsuma, T. Tanaka, S. Yoshida, T. Hattori, J. Synchrotron Radiat. 6 (1999) 471.
[39] B.C. Sales, J.E. Turner, M.B. Maple, Surf. Sci. 112 (1981) 272.
[40] V.P. Zhdanov, B. Kasemo, J. Catal. 220 (2003) 478.
[41] X.-Q. Gong, Z.-P. Liu, R. Raval, P. Hu, J. Am. Chem. Soc. 126 (2003) 8.